PNAS RESEARCH ARTICLE | EARTH, ATMOSPHERIC, AND PLANETARY SCIENCES
ANTHROPOLOGY OPEN ACCESS

Reconstructing biblical military campaigns using geomagnetic field data

Yoav Vaknin[a,b,1], Ron Shaar[b], Oded Lipschits[a], Amihai Mazar[c], Aren M. Maeir[d], Yosef Garfinkel[c], Liora Freud[a], Avraham Faust[e], Ron E. Tappy[f], Igor Kreimerman[c], Saar Ganor[g], Karen Covello-Paran[g], Omer Sergi[a], Zeev Herzog[a], Rami Arav[h], Zvi Lederman[a], Stefan Münger[i], Alexander Fantalkin[a], Seymour Gitin[j], and Erez Ben-Yosef[a]

Edited by Lisa Tauxe, University of California San Diego, La Jolla, CA; received May 27, 2022; accepted August 31, 2022

The Hebrew Bible and other ancient Near Eastern texts describe Egyptian, Aramean, Assyrian, and Babylonian military campaigns to the Southern Levant during the 10th to sixth centuries BCE. Indeed, many destruction layers dated to this period have been unearthed in archaeological excavations. Several of these layers are securely linked to specific campaigns and are widely accepted as chronological anchors. However, the dating of many other destruction layers is often debated, challenging the ability to accurately reconstruct the different military campaigns and raising questions regarding the historicity of the biblical narrative. Here, we present a synchronization of the historically dated chronological anchors and other destruction layers and artifacts using the direction and/or intensity of the ancient geomagnetic field recorded in mud bricks from 20 burnt destruction layers and in two ceramic assemblages. During the period in question, the geomagnetic field in this region was extremely anomalous with rapid changes and high-intensity values, including spikes of more than twice the intensity of today's field. The data are useful in the effort to pinpoint these short-term variations on the timescale, and they resolve chronological debates regarding the campaigns against the kingdoms of Israel and Judah, the relationship between the two kingdoms, and their administrations.

archaeomagnetism | archaeomagnetic spike | archaeomagnetic dating | chronology | archaeointensity

Significance

Studying the events described in the Hebrew Bible is a complex task that involves textual and archaeological investigation and often bears highly contentious results. Here, we introduce an approach that applies archaeomagnetic investigation to the remains of ancient towns that were destroyed by fire. The new magnetic data provided chronological insights that enabled linking archaeological contexts with specific military campaigns, shedding new light on the history of the biblical kingdoms of Israel and Judah. This interdisciplinary study also reconstructs the behavior of the geomagnetic field during a unique period in its history, when it changed rapidly and exceeded twice the intensity of today's field. This has significant implications for various fields of research, including geodynamic modeling in geophysics.

The Hebrew Bible and other ancient Near Eastern texts describe military campaigns against the kingdoms of Israel and Judah during the 10th to sixth centuries BCE. Specifically, the Aramean, Assyrian, and Babylonian military campaigns left behind destruction layers known from intensive archaeological excavations. However, only a few destruction layers are securely associated with specific historical campaigns thanks to a rare combination of historical and archaeological data. These are widely accepted as chronological anchors (1), sometimes accurately dated to a year or even a defined month or day (2, 3). The attribution of other destruction layers to specific campaigns is debated, posing challenges to reconstructing the scale and geographic span of the campaigns. Here we use archaeomagnetism as a complementary chronological tool in order to synchronize between the chronological anchors and other destruction layers and artifacts whose dating cannot be validated by radiocarbon or direct historical documentation.

Results

We reconstructed the direction and/or intensity of Earth's magnetic field recorded in 20 burnt destruction layers exposed at 17 archaeological sites and in two ceramic assemblages (*SI Appendix*, Tables S1–S6). From the destruction layers we sampled sun-dried mud bricks (*SI Appendix*, Fig. S1*A*), which had acquired thermoremanent magnetization (TRM) when the sites were destroyed by fire. In one case we sampled a kiln that had gone out of use when the site had been destroyed. The data, obtained from the analysis of 1,186 specimens from 144 samples, are shown in Fig. 1 along with our recent compilations of published data from the Levant and Western Mesopotamia (3–5). Fig. 1*A* also displays an archaeointensity curve (LAC.v.1.0) (5), constructed using a transdimensional Bayesian method (6) based on all these data (see *SI Appendix, Detailed Methods* and Fig. S2). Detailed results are presented in *SI Appendix*, Figs. S3–S9 and Tables S7, S8, S10, S12–S15. All the archaeomagnetic data, as well as the interpretations presented here, are available in the MagIC database (http://earthref.org/MagIC/19397).

Discussion

The concept of archaeomagnetic dating is based on comparing paleomagnetic direction and/or intensity from an archaeological feature or a collection of finds with a reference

Competing interest statement: Lisa Tauxe and R.S. are coauthors on two research articles published in 2019 and 2022, and Lisa Tauxe and E.B.-Y. are coauthors on a research article published in 2021.

This article is a PNAS Direct Submission.

[1]To whom correspondence may be addressed. Email: yoavvaknin@mail.tau.ac.il.

This article contains supporting information online at http://www.pnas.org/lookup/suppl/doi:10.1073/pnas.2209117119/-/DCSupplemental.

Published October 24, 2022.

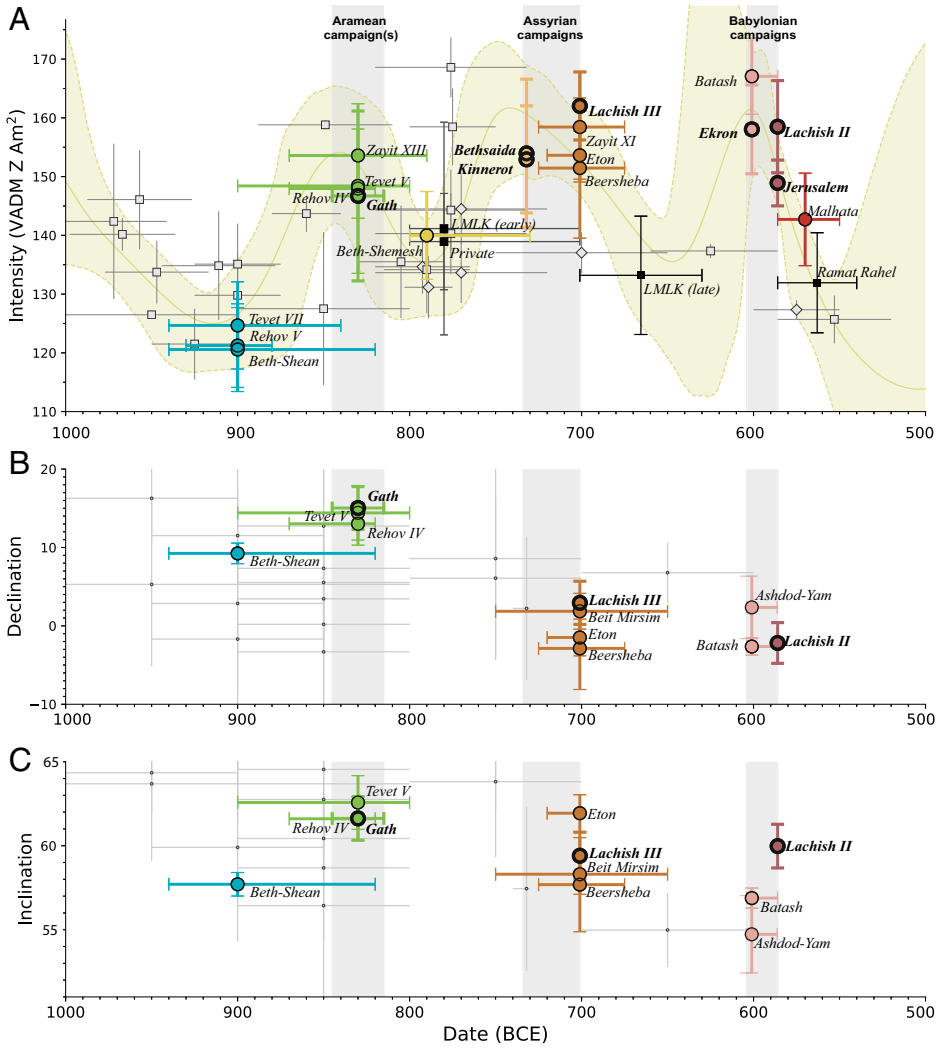

Fig. 1. Archaeomagnetic results. (*A*) Field intensity results shown with LAC.v.1.0 (5) displayed as the virtual axial dipole moment (VADM). (*B*) The angle between the horizontal component and the geographic north (Declination). (*C*) The angle from the horizontal plane (Inclination). All directions are relocated to Jerusalem. Results from destruction layers are represented by colored circles (for color key, see Fig. 3). Note that some destruction layers have only intensity (*A*) or direction (*B*–*C*) results. Intensity results from pottery discussed in the text are represented by black squares. Intensity data included in LAC.v.1.0 (5) from Israel (squares) and Syria (diamonds) are marked in gray. Previously published directions (3, 4) from the Levant are marked in gray dots. Chronological anchors are highlighted in bold. Note that the locations of the symbols on the time axis within the horizontal error bars were assigned arbitrarily, according to the different chronological considerations including the archaeomagnetic results. These assigned ages (*SI Appendix*, Tables S2–S6 and S9) are not considered as part of the prior data for the AH-RJMCMC model.

geomagnetic secular variation curve (7). According to one approach, a probability distribution of ages is calculated using a curve constructed independently from the object being dated (8–11). According to another approach, adopted here following Livermore et al. (6), the datum to be dated is included in the Bayesian procedure used to produce the curve (12–15). Another common practice that has been in use in the Levant (16–19) and is also applied here is the comparison of results from different sites in order to negate or support hypotheses of contemporaneity. The following analysis applies these concepts in order to shed light on several ongoing chronological debates, summarized in *SI Appendix*, Table S9.

According to historical sources, Hazael, King of Aram Damascus, led at least one military campaign to the Southern Levant and according to the Hebrew Bible (2 Kings 12:18) he destroyed Gath of the Philistines. This event left an extensive destruction layer and, based on historical and archaeological data including radiocarbon, there is a wide consensus that it should be dated to ca. 830 BCE (20), although the possibility that it occurred in 798 BCE was suggested in the past (21). Both the archaeomagnetic direction and intensity from Gath show outstanding agreement with three other destruction layers dated to the ninth century BCE (Fig. 1 and *SI Appendix*, Fig. S10): Tel Rehov Stratum IV (22), Horvat Tevet Level V (23), and Tel Zayit Level XIII (only intensity results were obtained) (24). Thus, the archaeomagnetic results strongly support the synchronization of these three destructions with that of Gath (Fig. 2), and we suggest that they were also the result of the Aramean campaign(s) of Hazael. This conclusion is demonstrated in the archaeomagnetic dating of Tel Zayit Level XIII (Fig. 3*C*), which narrows down its archaeological age range to approximately the age range of Gath's destruction.

Our study of a destruction layer in Tel Beth-Shean, a major city located only 5 km from Tel Rehov, demonstrates the application of archaeomagnetism to resolve a chronological debate. The excavator of the site suggested that Beth-Shean had been destroyed by either Pharaoh Shoshenq I (biblical Shishak) in ca. 920 BCE or by Hazael in the late ninth century BCE (25) and recently favored the later date (22). However, according to ceramic typology it could have been concurrent either with

Fig. 2. Map of the studied destruction layers and the different military campaigns. A schematic illustration of possible routes is presented following Rainey and Notley (21). Chronological anchors are highlighted in bold.

Stratum IV or with the earlier Stratum V at Tel Rehov, which included the destruction by fire of unique mud beehives and was dated by radiocarbon to ca. 900 BCE (22). Archaeomagnetic dating of Beth-Shean (Fig. 3*A*) shows that at a 95% confidence level the destruction occurred before ca. 880 BCE and at a 68% confidence level it occurred before ca. 900 BCE. The magnetic inclination of Beth-Shean is in agreement with this dating constraint, showing a difference of ~4° from the reference inclination of Gath, Rehov IV, and Tevet V and no overlap in their α_{95} confidence cones (Fig. 1*C* and

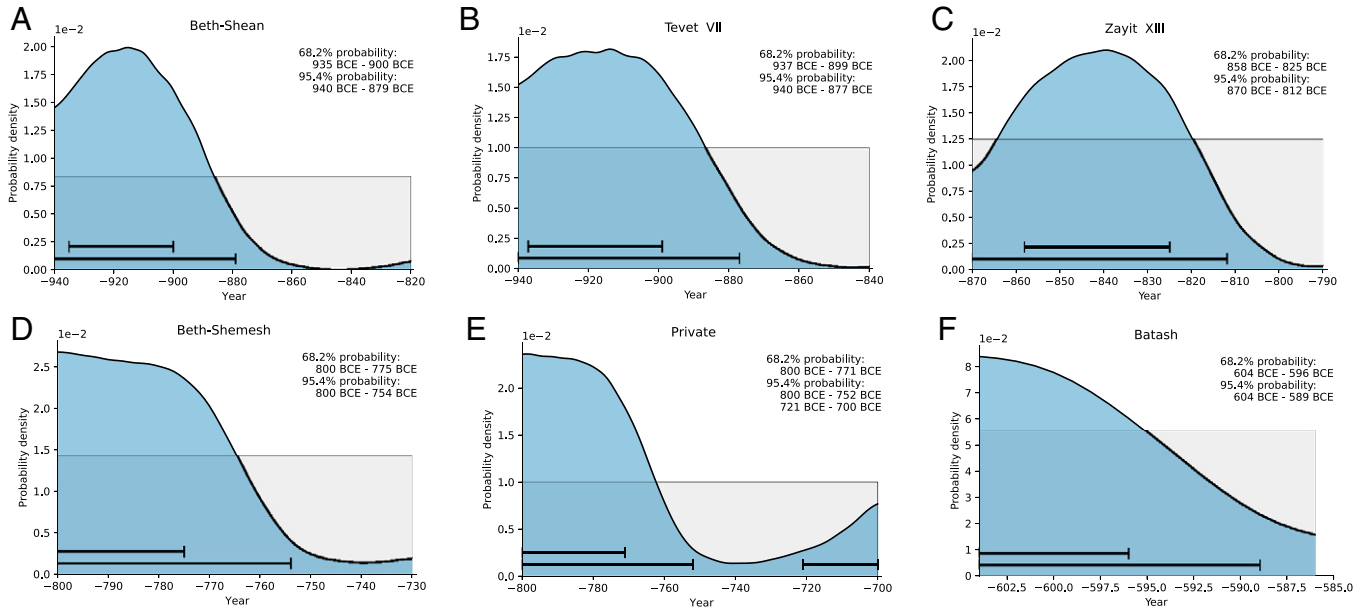

Fig. 3. Archaeomagnetic dating using archaeointensity marginalized dating (6). (*A*) Tel Beth-Shean. (*B*) Horvat Tevet Level VII. (*C*) Tel Zayit Level XIII. (*D*) Tel Beth-Shemesh. (*E*) "Private" stamped handles (42). (*F*) Tel Batash. The prior age range used by the AH-RJMCMC algorithm (6) is based on historical and archaeological considerations, including radiocarbon when available, and is represented as a uniform probability density function (gray background). The posterior age probability distribution is shown in blue.

SI Appendix, Fig. S10). Thus, we conclude that there must be a time gap between the destruction of Beth-Shean and that of Gath, Rehov IV, Tevet V, and Tel Zayit XIII.

The archaeointensity data (Fig. 1*A*) and the archaeomagnetic dating of Beth-Shean and Horvat Tevet Level VII (23) (Fig. 3 *A* and *B*) support the possibility that both sites were destroyed concurrently with the unique apiary in Stratum V at Tel Rehov, which was destroyed by fire in the late 10th to early ninth century BCE according to radiocarbon dating (22, 26). Historically, these three early destructions could be the result of the well-discussed and debated Egyptian campaign of Pharaoh Shoshenq I (26). Shoshenq's campaign is mentioned in the Hebrew Bible (2 Kings 14:25–26) and in his Triumphal Relief at Karnak (Egypt), where Rehov and Beth-Shean are depicted side by side as prisoners of war, each representing a conquered city.

A similar example of archaeomagnetic dating that sheds light on the historical interpretation of a destruction is the Judean city at Tel Beth-Shemesh. According to ceramic typology and radiocarbon dating, this destruction occurred after the times of Hazael's campaigns. Due to the plateau in the radiocarbon calibration curve (27), radiocarbon alone does not allow for high-resolution dating of this destruction. The excavators dated it to ca. 790 BCE and, based on the description in 2 Kings 14:11–13, attributed this destruction to Jehoash, King of Israel (28). According to our archaeointensity-derived age (Fig. 3*D*), the excavators' suggestion seems more probable than other suggestions that date the destruction to the middle of the eighth century BCE (1).

In 733 to 732 BCE, Tiglath-Pileser III, King of Assyria, conquered the northern parts of the Kingdom of Israel, as described in biblical and Assyrian sources. The attribution of the destructions at Bethsaida (29) and Tel Kinnerot (30) to this period is widely accepted. The agreement between our archaeointensity results from these two sites reinforces their concurrent destruction (Figs. 1*A* and 2). During another Assyrian campaign, led by King Sennacherib in 701 BCE, Tel Lachish Stratum III was destroyed. Unequivocal evidence of the siege, battle, and destruction by fire has been exposed at the site (2, 31). The attack on Lachish is mentioned in 2 Kings 18–19; Isaiah 36–37; 2 Chronicles 32 and narrated in Assyrian reliefs. According to biblical and Assyrian sources, many other Judean sites were destroyed during the 701 BCE campaign but none are securely identified. Our archaeomagnetic data from Tel Beersheba (32), Tel Zayit Level XI (24), and Tell Beit Mirsim (33) argue for their destruction during the 701 BCE campaign (Fig. 2). Despite the marginal overlap of inclination results from Tel Eton and Lachish III, the destruction of Tel Eton also presumably occurred during an Assyrian campaign of the late eighth century BCE (34).

After the Assyrian withdrawal from the Levant, the Babylonians conquered the region in several campaigns led by Nebuchadnezzar II. The exact date of destruction of the Philistine city of Ekron is debated, but it surely occurred during one of the Babylonian campaigns between 604 and 598 BCE (35, 36). The 586 BCE Babylonian campaign led to the destruction of Tel Lachish Stratum II (2, 37) and to the destruction of Jerusalem (3, 36) and its temple (2 Kings 24:18; Jeremiah 1:3; 39:2; 52:5–6), bringing the Kingdom of Judah to its end. Our direction results from Lachish II, based on an intact mud–brick wall, represent the geomagnetic direction in 586 BCE more accurately and precisely than a previous estimation that was based on collapsed material from Jerusalem (3). There is a difference of ~3° in inclination between the destruction of Batash and that of Lachish II, and the α_{95} confidence cones of these two sites do not overlap (Fig. 1*C*). Furthermore, our intensity results from Tel Batash overlap with those from neighboring Ekron but not with those from the 586 BCE destruction of Jerusalem (Fig. 1*A*). Therefore, the archaeomagnetic intensity results, with some possible support from the direction results, suggest that Batash, like Ekron, was destroyed by the Babylonians in ca. 600 BCE (Figs. 2 and 3F), perhaps in 604 BCE as the excavator assumed (38) and not during the 586 BCE campaign as has recently been suggested (39). The direction results from Ashdod-Yam (40) may suggest that it too was destroyed in ca. 600 BCE.

The intensity results from Tel Malhata (41) are slightly lower than those recorded in Lachish II. This supports the hypothesis (39) that in 586 BCE the Babylonian army was focused on Jerusalem and had no interest in going far south to the area of Malhata. It seems that after 586 BCE, when the Kingdom of Judah ceased to exist, the eastern and southern periphery of the kingdom collapsed, probably in a gradual process, and sites were destroyed, perhaps by the Edomites or other nomadic elements (Fig. 2). The Edomite threat to the collapsing Judean kingdom is reflected in the Hebrew Bible and in a few ostraca discovered in Arad and Horvat Uza (36).

Our large, well-dated dataset enabled revisiting the debated dating of two sets of stamped storage jar handles that were part of the administrative system of the Kingdom of Judah (39): an early subset of LMLK handles (meaning in Hebrew "belonging to the king") and the "private" stamped handles bearing names, probably of officials. Since these two sets were found in destruction layers dated to 701 BCE and not in later contexts, it is accepted that they were in use until 701 BCE (39). However, the introduction date of these sets is debated. It has recently been suggested that their introduction was after the 733 to 732 BCE Assyrian campaigns, a suggestion based mainly on historical assumption and on the fact that no handles of these types were found in destruction layers from the Kingdom of Israel that are attributed to these campaigns (39). However, comparing our results from the destruction layers to previous archaeointensity measurements from handles of both types (42) and to measurements from four LMLK handles reported here (*SI Appendix*, Tables S1, S6, S8, and S15) supports an even earlier introduction. Due to the similar intensity results from all six destruction layers dated to 733 to 701 BCE, it seems unlikely that the field intensity changed considerably during this short period. The intensity results of all measured "private" handles and some of the early LMLK handles are lower than the field recorded during the 733 to 701 BCE campaigns and are in agreement with published data from the first half of the eighth century BCE. Following these results, as demonstrated in the archaeomagnetic dating of the "private" stamped handles (Fig. 3*E*), we suggest that both sets could have already been in use during the first half of the eighth century BCE. This suggestion is relevant to the debate regarding the appearance of a complex polity in Judah. The absence of these Judean handles from the 733 to 732 BCE destruction layers in the Kingdom of Israel should not be regarded as a chronological constraint. It can be understood in the context of the rivalry between the two kingdoms, as reflected in biblical narratives regarding the destruction of Beth-Shemesh mentioned above and the unsuccessful Israelite attack on Judah in the attempt to force the kingdom to join the anti-Assyrian coalition (2 Kings 16:5–8) (21).

During the investigated period, the geomagnetic field in the Levant was anomalous compared to the past several millennia, with high field intensity values reaching twice the intensity of today's field, angular deviations from the averaged direction, and a fast secular variation rate (4, 5, 42–45). The precisely dated data reported here constrain the evolution of the Levantine geomagnetic anomaly and are an essential part of the new LAC.v.1.0 reported in Shaar et al. 2022 (5). In particular, our results point to the existence of a hitherto unrecognized spike in ca. 600 BCE (Fig. 1). This spike came after a relatively weak field during the seventh century BCE, as represented in the late LMLK stamped handle group, and was followed by a rapid decrease, reinforced by new data from Tel Malhata and Ramat Rahel (46) (*SI Appendix*, Table S8).

This research demonstrates how an archaeointensity curve constructed from a dense archaeomagnetic dataset in which the chronology rests on radiocarbon (for periods before the eighth century BCE) and firm historical ages (from the eighth century BCE and on) can be used as a powerful chronological tool. This is especially useful during the Hallstatt Plateau (ca. 800–400 BCE) (27), a period in which the resolution of radiocarbon dating is limited. This research also demonstrates the direct applicability of archaeomagnetism to solving questions related to the synchronization of archaeological contexts, especially its potential to negate concurrency. The Aramean, Assyrian, and Babylonian campaigns turned out to have occurred at times of very high geomagnetic field intensity and are separated by well-defined minima. This should also be very useful for future dating efforts, distinguishing these major campaigns from other periods in the history of the Levant.

Materials and Methods

Archaeomagnetic Groups and Features and Their Ages. *SI Appendix*, Table S1 lists the names and locations of all the archaeomagnetic groups analyzed for archaeointensity and the archaeomagnetic features analyzed for archaeomagnetic direction. *SI Appendix*, Tables S2–S6 present detailed archaeological data regarding these features and archaeomagnetic groups including their ages. These age ranges are based on historical and archaeological considerations including radiocarbon, when available, as presented in *SI Appendix*, Tables S2–S6. In cases in which the dating is debated, we assigned a wide age range that covers the different possible options. For this reason we revised previously published dates by extending the age range of the early LMLK stamped handles from the maximum age range (750–701 BCE) suggested in a previous publication (42) to 800 to 701 BCE. Since it is widely accepted (39) that the "private" handles were in use until 701 BCE, we set the age range for this group to 800 to 701 BCE as well. An additional file attached to the *SI Appendix* includes additional archaeological information regarding the sampled features and archaeomagnetic groups including pictures of the sampled materials.

Archaeointensity. In most cases we sampled burnt mud bricks for archaeointensity experiments, with several exceptions. In Stratum V at Tel Rehov we sampled a beehive made of mud that had been burned during the destruction of the apiary. In Level XIII in Tel Zayit we sampled, in addition to two burnt mud bricks, a loom weight (or fermentation stopper) and a jar lid, both originally made of unburnt clay and presumably burned during the destruction. In two cases we measured a group of pottery vessels in order to reconstruct the intensity of the field during periods not represented by destruction layers: a ceramic assemblage from Ramat Rahel (46) (labeled sh3e; see *SI Appendix*, Table S8) and four stamped handles from the late subset of the LMLK (labeled lmlk_late; see *SI Appendix*, Table S8), which belong to the late LMLK group reported in Ben-Yosef et al. (42).

Specimens for archaeointensity experiments were prepared from unoriented samples, where a sample denoted a single brick in the case of burnt structures or a single pottery vessel in the case of the indicative pottery fragments collected from Ramat Rahel. Specimen sizes ranged from ca. $5 \times 5 \times 5$ mm to ca. $13 \times 13 \times 13$ mm. Prior to the experiments, we heated empty squared alumina crucibles ($2 \times 2.2 \times 2.2$ cm in size) to 600 °C in a 60 μT field and measured their TRM. Only crucibles with TRM lower than 10^{-10}Am^2 (three to four orders of magnitude weaker than our typical specimen) were used. The specimens were then glued into the alumina crucibles.

Archaeointensity experiments were carried out at the magnetically shielded paleomagnetic laboratory at the Institute of Earth Sciences at the Hebrew University of Jerusalem, using a 2G Enterprises RAPID superconducting rock magnetometer (SRM) system and two laboratory-modified, computer-controlled ASC-TD48 ovens. Thellier-type paleointensity experiments were carried out following the IZZI protocol (47, 48), with partial TRM (pTRM) checks (49) at every second temperature step, at progressively elevated temperatures, from 100 °C up to 600 °C or until the natural remanent magnetization (the recorded magnetization) was fully demagnetized. The Thellier-type paleointensity experiments typically included

15 temperature steps. Anisotropy experiments included eight steps at the maximum temperature reached during the Thellier–IZZI experiment (usually 600 °C): a demagnetization step, six TRM acquisition steps at orthogonal orientations (+x, −x, +y, −y, +z, −z), and an alteration check step (*SI Appendix*, Fig. S4 *A* and *C*). Cooling rate experiments included four steps: fast rate (fan-cooled); two slow exponentially cooled steps with a cooling function $T = RT + (T_0 - RT)e^{-At}$, where RT represents room temperature and $A = 0.003$, 0.001 for slow, and very slow rates, respectively; and an alteration check at the fast rate (*SI Appendix*, Figs. S3*B* and S4 *B* and *C*).

Data analysis was done using the PmagPy Thellier GUI program (50, 51), applying the automatic interpretation algorithm (45) and the same acceptance criteria used for the entire set of LAC.v.1.0 data (5, 52) (*SI Appendix*, Fig. S2 and Table S11). The archaeointensity means of the burnt structures (termed here "groups") and pottery groups were calculated by averaging the STDEV-OPT means (50) of individual bricks, artifacts, or pottery fragments (termed here "samples"), where each sample mean is based on results from three to 15 specimens. For a detailed description of the calculation algorithm, see Shaar et al. 2020 (52).

Archaeomagnetic Directions. Archaeomagnetic directions were all obtained from oriented hand samples collected from archaeomagnetic features. These features were usually burnt mud brick walls, with the exception of a kiln from Horvat Tevet Stratum V, which went out of use following the destruction of this stratum. When the burnt mud bricks that were unearthed collapsed (Beersheba_collapse, Beth-Shemesh_collapse, Tevet_collapse, Gath_collapse_Area_A, Gath_collapse_Area_M; *SI Appendix*, Table S1), we sampled them in situ for site formation analysis only, i.e., to find out whether they had cooled down in the orientation in which they were exposed (3) (*SI Appendix*, Table S10). Measurements from these collapsed bricks were not used to reconstruct the direction of the ancient field.

Prior to sampling, we polished the surface of the bricks in order to create flat surfaces. Bricks that tended to crumble were sprayed with nonmagnetic potassium silicate glue in order to prevent disintegration. If the surface of the mud bricks was rough, due to cavities left by straw that had been added to the mud–brick matrix during construction, then we applied a thin layer of plaster of Paris in order to create flat surfaces (*SI Appendix*, Fig. S1*B*). On the flat surfaces we marked horizontal lines (*SI Appendix*, Fig. S1*A*) and measured their strike and dip. The strike was measured using a device we developed for this research (*SI Appendix*, Fig. S1*C*) that enables measuring the orientation using both a sun compass and a Brunton magnetic compass. This device was designed so that the magnetic compass would be located approximately 15 cm away from the measured surface in order to reduce the possible effect of the magnetic field of the burnt bricks on the compass. The oriented samples taken from the outer surfaces of the bricks (termed hereafter "samples") were cut into smaller specimens in the laboratory. By cutting one edge of every specimen parallel to the strike, we managed to maintain its orientation measurements. The specimens were then glued in nonmagnetic paleomagnetic sampling boxes, 19 × 23 × 23 mm in size.

Demagnetization experiments were carried out at the magnetically shielded paleomagnetic laboratory at the Institute of Earth Sciences at the Hebrew University of Jerusalem, using a 2G Enterprises RAPID SRM system with an in-line 2-axis alternating field demagnetizer. Demagnetization experiments were carried out at progressively elevated peak fields in 4 mT steps up to 20 mT, 5 mT steps up to 40 mT, 10 mT steps up to 70 mT, and 15 mT steps up to 100 mT. Data were analyzed using PmagPy Demag-GUI (51) following Kirschvink (53). Archaeomagnetic feature means were calculated following Fisher (54).

Archaeomagnetic Dating. Archaeomagnetic ages were obtained using the AH-RJMCMC algorithm described in Livermore et al. (6). The algorithm uses all data in the LAC.v.1.0 compilation (5) as its prior information. These data include the following: intensity values of the different archaeointensity groups modeled as a Gaussian, age ranges of the groups modeled as a uniform distribution or a Gaussian in case of direct radiocarbon dating, and stratigraphic order (when applicable). All prior ages are based on radiocarbon data when available, on historical constraints when applicable, and on archaeological considerations. Nonanalytic archaeological age ranges are generally wider and include all the possible corrections to absolute timescales. Archaeomagnetic data are not considered in the prior ages to prevent circular reasoning. The output of the AH-RJMCMC technique is an age posterior distribution for each of the LAC.v.1.0 data, from which we extracted the 68.2% and 95.4% credible intervals for selected groups (Fig. 3).

Rock Magnetism Thermomagnetic curves of magnetic susceptibility (*SI Appendix*, Fig. S8) were measured using an AGICO MFK-1 Kappabridge with a CS4 furnace. The magnetic susceptibility was measured in repeated heating cycles at progressively elevated peak temperatures, up to 700 °C. Magnetic hysteresis and first-order reversal curve (FORC) measurements were carried out using a Lakeshore 8604 vibrating sample magnetometer and analyzed using the FORCinel program (55). The FORC diagrams were calculated from 600 equally spaced loops measured with a saturation field of 1 T and an averaging time of 100 mT and using the following VARIFORC smoothing parameters (56): $s_{c,0} = 3$, $s_{c,1} = 7$, $s_{b,0} = 4$, $s_{b,1} = 7$.

Data, Materials, and Software Availability. Archaeomagnetic data have been deposited in the MagIC database (http://earthref.org/MagIC/19397) (57).

ACKNOWLEDGMENTS. We are grateful to the team members of the archaeological excavations for all their support in the fieldwork and beyond. We thank Phil Livermore for his assistance with the AH-RJMCMC analysis. We thank Yael Ebert, Lilach Gonen, Lior Bar, Erez Hassul, and Yakar Zemach for their assistance in the paleomagnetic laboratory. We further acknowledge Sherry and Vernon Whetstone, Vladik Lipshits, Itamar Weissbein, Yoav Zur, and Miriam Lavi for their help in sampling. We thank Yves Gallet, Jacob Schreibman, Assaf Kleiman, Hoo-Goo Kang, Shifra Weiss, Yosef Stepansky, David Ussishkin, Omri Yagel, and Eli Itkin for their helpful advice. We appreciate the fruitful discussions regarding this research with Nava Panitz-Cohen, Naama Yahalom-Mack, and Yves Gallet. We thank Itamar Ben-Ezra for helping us to prepare the figures (Figs. 1–3). We thank two anonymous reviewers for all their constructive comments that significantly improved the quality of this paper. This project has received funding from the European Research Council under the European Union's Horizon 2020 research and innovation program (grant agreement no. 804490) to R.S. The study was partly supported by Israel Science Foundation grant 1364/15 to R.S. This publication was also supported by the Chaim Rosenberg School of Jewish Studies-Archaeology, Tel Aviv University.

Author affiliations: [a]Institute of Archaeology, Tel Aviv University, Tel Aviv 69978, Israel; [b]Institute of Earth Sciences, The Hebrew University of Jerusalem, Jerusalem 9190401, Israel; [c]Institute of Archaeology, The Hebrew University of Jerusalem, Jerusalem 9190501, Israel; [d]Institute of Archaeology, The Martin (Szusz) Department of Land of Israel Studies and Archaeology, Bar-Ilan University, Ramat Gan 590002, Israel; [e]Department of General History, Bar-Ilan University, Ramat Gan 590002, Israel; [f]Pittsburgh Theological Seminary, Pittsburgh, PA 15206; [g]Israel Antiquities Authority, Jerusalem 9100402, Israel; [h]University of Nebraska Omaha, Omaha, NE 68182; [i]Institute of Jewish Studies, University of Bern, Bern 3012, Switzerland; and [j]W.F. Albright Institute of Archaeological Research, Jerusalem 9119002, Israel

Author contributions: Y.V., R.S., O.L., and E.B.-Y. designed research; Y.V., R.S., and E.B.-Y. performed research; O.L., A.M., A.M.M., Y.G., L.F., A. Faust, R.E.T., I.K., S. Ganor, K.C.-P., O.S., Z.H., R.A., Z.L., S.M., A. Fantalkin, and S. Gitin conducted archaeological excavations and provided samples; Y.V. and R.S. analyzed data; Y.V., R.S., O.L., and E.B.-Y. wrote the paper and all coauthors reviewed previous drafts; and Y.V., R.S., O.L., A.M.M., and E.B.-Y. reviewed the final version.

1. I. Finkelstein, E. Piasetzky, Radiocarbon-dated destruction layers: A skeleton for Iron Age chronology in the Levant. *Oxf. J. Archaeol.* **28**, 255–274 (2009).
2. D. Ussishkin, The *Renewed Archaeological Excavations* at Lachish (1973-1994) (Monograph Series of the Sonia and Marco Nadler Institute of Archaeology, Emery and Claire Yass Publications in Archaeology, Tel-Aviv, Israel, 2004).
3. Y. Vaknin *et al.*, The Earth's magnetic field in Jerusalem during the Babylonian destruction: A unique reference for field behavior and an anchor for archaeomagnetic dating. *PLoS One* **15**, e0237029 (2020).
4. R. Shaar *et al.*, The first catalog of archaeomagnetic directions from Israel with 4000 years of geomagnetic secular variations. *Front. Earth Sci.* **6**, 164 (2018).
5. R. Shaar *et al.*, Archaeomagnetism in Levant and Mesopotamia reveals the largest changes in the geomagnetic field. ESSOAr [Preprint] (2022). https://www.essoar.org/doi/10.1002/essoar.10511816.2 (Accessed 20 September 2022).
6. P. W. Livermore, A. Fournier, Y. Gallet, T. Bodin, Transdimensional inference of archeomagnetic intensity change. *Geophys. J. Int.* **215**, 2008–2034 (2018).
7. J. L. Eighmy, R. S. Sternberg, *Archaeomagnetic Dating* (University of Arizona Press, 1990).
8. P. Lanos, "Bayesian inference of calibration curves: Application to archaeomagnetism" in *Tools for Constructing Chronologies: Crossing Disciplinary Boundaries*, C. E. Buck, A. R. Millard, Eds. (Springer London, London, UK, 2004), pp. 43–82.

9. F. Pavon-Carrasco, J. Rodrigues-Gonzalez, M. L. Osete, J. M. Torta, A Matlab tool for archaeomagnetic dating. *J. Archaeol. Sci.* **38**, 408–419 (2011).
10. L. Casas, E. Tema, Investigating the expected archaeomagnetic dating precision in Europe: A temporal and spatial analysis based on the SCHA.DIF.3K geomagnetic field model. *J. Archaeol. Sci.* **108**, 104972 (2019).
11. Á. Herrejón-Lagunilla *et al.*, Dating a medieval pottery workshop of the city of Burgos (Spain): Archaeomagnetic and archaeological evidences. *Phys. Earth Planet. Inter.* **316**, 106723 (2021).
12. E. Schnepp, M. Obenaus, P. Lanos, Posterior archaeomagnetic dating: An example from the Early Medieval site Thunau am Kamp, Austria. *J. Archaeol. Sci. Rep.* **2**, 688–698 (2015).
13. G. Hervé, P. Lanos, Improvements in archaeomagnetic dating in Western Europe from the Late Bronze to the Late Iron Ages: An alternative to the problem of the Hallstattian Radiocarbon Plateau. *Archaeometry* **60**, 870–883 (2018).
14. Y. Gallet, M. Fortin, A. Fournier, M. Le Goff, P. Livermore, Analysis of geomagnetic field intensity variations in Mesopotamia during the third millennium BC with archeological implications. *Earth Planet. Sci. Lett.* **537**, 116183 (2020).
15. A. Genevey *et al.*, Archeomagnetic intensity investigations of French medieval ceramic workshops: Contribution to regional field modeling and archeointensity-based dating. *Phys. Earth Planet. Inter.* **318**, 106750 (2021).
16. E. Ben-Yosef *et al.*, A new approach for geomagnetic archaeointensity research: Insights on ancient metallurgy in the southern Levant. *J. Archaeol. Sci.* **35**, 2863–2879 (2008).
17. E. Ben-Yosef, L. Tauxe, T. E. Levy, Archaeomagnetic dating of copper smelting site F2 in Timna Valley (Israel) and its implication on modeling ancient technological developments. *Archaeometry* **52**, 1110–1121 (2010).
18. R. Shahack-Gross *et al.*, Fire and collapse: Untangling the formation of destruction layers using archeomagnetism. *Geoarchaeology* **33**, 513–528 (2018).
19. M. Stillinger, J. Hardin, J. Feinberg, J. Blakely, Archaeomagnetism as a complementary dating technique to address the Iron Age chronology debate in the Levant. *Near East. Archaeol.* **79**, 90–106 (2016).
20. A. Maeir, "Introduction and overview" in *Tell es-Safi/Gath II: Excavations and Studies*, A. Maeir, J. Uziel, Eds. (Zaphon, Münster, Germany, 2020), pp. 1–52.
21. A. F. Rainey, R. S. Notley, *Carta's New Century Handbook and Atlas of the Bible* (Carta, Jerusalem, Israel, 2007).
22. A. Mazar, N. Panitz-Cohen, *Tel Reḥov: A Bronze and Iron Age city in the Beth-Shean Valley* (Qedem, Monographs of the Institute of Archaeology of the Hebrew University, Institute of Archaeology, Hebrew University of Jerusalem, Jerusalem, Israel, 2020), **vols. 1–5**.
23. O. Sergi, H. Bezzel, Y. Tsur, K. Covello-Paran, "Ḥorvat ṭevet in the Jezreel Valley: A royal Israelite estate" in *New Studies in the Archaeology of Northern Israel*, K. Covello-Paran, A. Erlich, R. Beeri, Eds. (The Israel Antiquities Authority, Jerusalem, Israel, 2021), pp. 31–48.
24. R. E. Tappy, The depositional history of Iron Age Tel Zayit: A response to Finkelstein, Sass, and Singer-Avitz. *Eretz-Israel (A. Ben-Tor Volume)* **30**, 127–143 (2011).
25. A. Mazar, "Beth-Shean from the late bronze age IIB to the medieval period: A summary" in *Excavations at Tel Beth-Shean, 1989-1996 I*, A. Mazar, Ed. (The Israel Exploration Society; The Institute of Archaeology, Hebrew University of Jerusalem, Jerusalem, Israel, 2006), pp. 26–47.
26. H. J. Bruins, J. van der Plicht, A. Mazar, 14C dates from Tel Rehov: Iron-Age chronology, pharaohs, and Hebrew kings. *Science* **300**, 315–318 (2003).
27. P. J. Reimer *et al.*, The IntCal20 northern hemisphere radiocarbon age calibration curve (0–55 cal kBP). *Radiocarbon* **62**, 725–757 (2020).
28. S. Bunimovitz, Z. Lederman, *Tel Beth-Shemesh: A Border Community in Judah: Renewed Excavations 1990–2000 I: The Iron Age* (Monograph Series of the Sonia and Marco Nadler Institute of Archaeology, Eisenbrauns, Winona Lake, IN, and Emery and Claire Yass Publications in Archaeology, Tel Aviv, Israel, 2016).
29. R. Arav, *Bethsaida: A City by the North Shore of the Sea of Galilee*, R. A. Freund, Ed. (Truman State University Press, 2009), vol. 4.
30. V. Fritz, Kinneret: Excavations at Tell El-'Oreimeh (Tel Kinrot) 1982-1985 seasons. *Tel Aviv* **20**, 187–215 (1993).
31. S. Ganor, I. Kreimerman, An eighth-century B.C.E. gate shrine at Tel Lachish, Israel. *Bull. Am. Schools Orient. Res.* **381**, 211–236 (2019).
32. Z. Herzog, L. Singer-Avitz, *Beer-Sheba III: The Early Iron IIA Enclosed Settlement and the Late Iron IIA-Iron IIB Cities* (Monograph Series of the Sonia and Marco Nadler Institute of Archaeology, Emery and Claire Yass Publications in Archaeology, Tel Aviv University, Tel Aviv, Israel, and Eisenbrauns, Winona Lake, IN, 2016).
33. O. Zimhoni, The Iron Age pottery of Tel 'Eton and its relation to the Lachish, Tell Beit Mirsim and Arad assemblages. *Tel Aviv* **12**, 63–90 (1985).
34. A. Faust *et al.*, The birth, life and death of an Iron Age house at Tel 'Eton, Israel. *Levant* **49**, 136–173 (2017).
35. D. B. MacKay, *Report of the 1994 Spring Excavations Field IISW: The Olive Oil Industrial Zone of the Late Iron Age II: Text, Data Base and Plates*, T. Dothan, S. Gitin, T. Miqne-Ekron, Eds. (W. F. Albright Institute of Archaeological Research, Jerusalem, Israel, 1995).
36. O. Lipschits, *The Fall and Rise of Jerusalem: Judah Under Babylonian Rule* (Eisenbrauns, Winona Lake, IN, 2005).
37. Y. Garfinkel *et al.*, The Canaanite and Judean cities of Lachish, Israel: Preliminary report of the Fourth Expedition, 2013–2017. *Am. J. Archaeol.* **125**, 419–459 (2021).
38. A. Mazar, Timnah (Tel Batash) I, Stratigraphy and Architecture, *Qedem* (Institute of Archaeology, Hebrew University of Jerusalem, Jerusalem, Israel, 1997).
39. O. Lipschits, *Age of Empires: The History and Administration of Judah in the 8th-2nd Centuries BCE in Light of the Storage-Jar Stamp Impressions* (Eisenbrauns, University Park, Pennsylvania, and Emery and Claire Yass Publications in Archaeology, The Institute of Archaeology, Tel Aviv University, Tel Aviv, Israel, 2021).
40. A. Fantalkin, "Neo-Assyrian involvement in the southern coastal plain of Israel: Old concepts and new interpretations" in *The Southern Levant Under Assyrian Domination*, A. Faust, S. Z. Aster, Eds. (Eisenbrauns, University Park, PA, 2018), pp. 162–185.
41. I. Beit-Arieh, L. Freud, *Tel Malḥata: A Central City in the Biblical Negev* (Eisenbrauns, Winona Lake, IN, 2015).
42. E. Ben-Yosef, M. Millman, R. Shaar, L. Tauxe, O. Lipschits, Six centuries of geomagnetic intensity variations recorded by royal Judean stamped jar handles. *Proc. Natl. Acad. Sci. U.S.A.* **114**, 2160–2165 (2017).
43. E. Ben-Yosef *et al.*, Geomagnetic intensity spike recorded in high resolution slag deposit in southern Jordan. *Earth Planet. Sci. Lett.* **287**, 529–539 (2009).
44. R. Shaar *et al.*, Geomagnetic field intensity: How high can it get? How fast can it change? Constraints from Iron Age copper slag. *Earth Planet. Sci. Lett.* **301**, 297–306 (2011).
45. R. Shaar *et al.*, Large geomagnetic field anomalies revealed in Bronze and Iron Age archaeomagnetic data from Tel Megiddo and Tel Hazor, Israel. *Earth Planet. Sci. Lett.* **442**, 173–185 (2016).
46. L. Freud, "The pottery assemblage" in *Ramat Raḥel VI: The Renewed Excavations by the Tel Aviv-Heidelberg Expedition (2005–2010). The Babylonian-Persian Pit*, O. Lipschits, L. Freud, M. Oeming, Y. Gadot, Eds. (Monograph Series of the Sonia and Marco Nadler Institute of Archaeology, Tel Aviv University, Tel Aviv, Israel, and Eisenbrauns, University Park, PA, 2021), pp. 28–72.
47. L. Tauxe, H. Staudigel, Strength of the geomagnetic field in the Cretaceous Normal Superchron: New data from submarine basaltic glass of the Troodos Ophiolite. *Geochem. Geophys. Geosyst.* **5**, Q02H06 (2004).
48. Y. Yu, L. Tauxe, A. Genevey, Toward an optimal geomagnetic field intensity determination technique. *Geochem. Geophys. Geosyst.* **5**, Q02H07 (2004).
49. R. S. Coe, S. Grommé, E. A. Mankinen, Geomagnetic paleointensities from radiocarbon-dated lava flows on Hawaii and the question of the Pacific nondiple low. *J. Geophys. Res.* **83**, 1740–1756 (1978).
50. R. Shaar, L. Tauxe, G. U. I. Thellier, An integrated tool for analyzing paleointensity data from Thellier-type experiments. *Geochem. Geophys. Geosyst.* **14**, 677–692 (2013).
51. L. Tauxe *et al.*, PmagPy: Software package for paleomagnetic data analysis and a bridge to the Magnetics Information Consortium (MagIC) Database. *Geochem. Geophys. Geosyst.* **17**, 2450–2463 (2016).
52. R. Shaar *et al.*, Synchronizing geomagnetic field intensity records in the Levant between the 23rd and 15th centuries BCE: Chronological and methodological implications. *Geochem. Geophys. Geosyst.* **21**, e2020GC009251 (2020).
53. J. L. Kirschvink, The least-squares line and plane and the analysis of palaeomagnetic data. *Geophys. J. R. Astr. Soc.* **62**, 699–718 (1980).
54. R. A. Fisher, Dispersion on a sphere. *Proc. R. Soc. Lond. A Math. Phys. Sci.* **217**, 295–305 (1953).
55. R. J. Harrison, J. M. Feinberg, FORCinel: An improved algorithm for calculating first-order reversal curve distributions using locally weighted regression smoothing. *Geochem. Geophys. Geosyst.* **9**, Q05016 (2008).
56. R. Egli, VARIFORC: An optimized protocol for calculating non-regular first-order reversal curve (FORC) diagrams. *Global Planet. Change* **110**, 302–320 (2013).
57. Y. Vaknin *et al.*, Data from "Reconstructing biblical military campaigns using geomagnetic field data." Magnetics Information Consortium. http://earthref.org/MagIC/19397.